

# RSC Advances



This is an *Accepted Manuscript*, which has been through the Royal Society of Chemistry peer review process and has been accepted for publication.

*Accepted Manuscripts* are published online shortly after acceptance, before technical editing, formatting and proof reading. Using this free service, authors can make their results available to the community, in citable form, before we publish the edited article. This *Accepted Manuscript* will be replaced by the edited, formatted and paginated article as soon as this is available.

You can find more information about *Accepted Manuscripts* in the [Information for Authors](#).

Please note that technical editing may introduce minor changes to the text and/or graphics, which may alter content. The journal's standard [Terms & Conditions](#) and the [Ethical guidelines](#) still apply. In no event shall the Royal Society of Chemistry be held responsible for any errors or omissions in this *Accepted Manuscript* or any consequences arising from the use of any information it contains.

Enhancement of the catalytic activity of ordered mesoporous TiO<sub>2</sub> by using carbon fiber support and appropriate evaluation of synergy between surface adsorption and photocatalysis by Langmuir–Hinshelwood (L–H) integration equation

Xiao Lin<sup>1</sup>, Ming Li<sup>2</sup>, Youji Li<sup>1,2\*</sup>, Wei Chen<sup>1</sup>

<sup>1</sup>College of Chemistry and Chemical Engineering, Jishou University, Hunan 416000, China

<sup>2</sup>Key laboratory of mineral cleaner production and exploit of green functional materials in hunan province, jishou university, 416000, China

**ABSTRACT** Ordered mesoporous titania on carbon fibers (OMT/CFs) were prepared through a simply combined method of liquid crystal template (LCT) technique and supercritical deposition. The OMT/CFs composites were characterized by scanning electron microscopy, transmission electron microscopy, x-ray diffraction, uv–vis diffuse reflectance spectroscopy, nitrogen adsorption–desorption isotherms, x-ray photoelectron spectroscopy (XPS) and photoluminescence (PL) emission spectra. These superiorities about small crystalline size, low exciton recombination, numerous activated sites, high hydroxy content and surface areas of OMT/CFs demonstrated functional property with remarkable enhanced degradation efficiency and adsorption capability on AO7 in comparison with nanostructured titania on CFs (NST/CFs) without LCT. Additionally, the OMT/CFs system also exhibited high photocatalytic activity in the repeating application. The photoactivities of OMT/CFs and NST/CFs are higher than those of OMT–CF and NST–CF physical mixtures due to tight combination resulting high synergistic effect of an acid orange 7 (AO7) degradation. This study showed that it is not appropriate to approximate the Langmuir–Hinshelwood (L–H) kinetics to first-order kinetics to evaluate synergy. The synergistic effect estimated by the ratio of apparent rate constant from first-order kinetics is generally increased because its rate constant

\* Corresponding author: Tel.: +86–13762157748; fax: +86–0743–8563911.  
E-mail address: bcelyj@163.com (Y.J. Li)

includes the adsorption effect. It is also proved that the decrease of AO7 content in solution is simultaneously attributed to adsorption of carbon fiber support besides its degradation in photocatalytic process. So the synergistic effect is inaccurate by evaluation of the approximated L–H model. To eliminate the adsorption influence of the catalyst, a L–H integration equation is proposed and found to well describe the photocatalytic behavior and evaluate synergistic effect, which is also verified by AO7 transfer on CFs and adsorption contribution.

**Keywords:** Ordered mesoporous titania, Carbon fiber, Synergy, Supercritical, Liquid crystal template

## 1. Introduction

Titanium dioxide, a chemically stable, highly efficient, nontoxic, and relatively inexpensive photocatalyst, has been widely used for water and air purification because many environmental pollutants can be degraded by decomposition and oxidation processes on its surface [1–4]. However, its high fineness, poor absorption of pollutants, and difficulty of recovery from water have hindered its application in photocatalysis [5,6]. An effective strategy has been applied to overcome the aforementioned shortcomings. Porous materials are ideal catalyst supports because of their large surface area. In addition, their uniform pore size distribution permits easy diffusion of large organic molecules toward internal active sites. Some researchers have developed porous material supported TiO<sub>2</sub> as efficient photocatalysts and successfully increased absorption including ceramic, glass and metal using various techniques [7–11]. Porous carbon (PC) is widely used as a support for TiO<sub>2</sub> in gas and water remediation because of its good adsorption properties. TiO<sub>2</sub> supported on PC exhibits a synergism that markedly enhances the kinetics of photodegradation of pollutants [2,12–14]. Among PC, carbon fibers (CFs), as an adsorbent has recently received increasing attention because of its high surface area, high adsorption capacity, and suitable pore structure [15,16], are therefore amenable for use as catalyst support for various purposes [17–19].

Efficient oxidation of organics requires adsorption onto the TiO<sub>2</sub> surface because the photocatalytic process is surface-orientated [20–22]. It is well known that the effectiveness of titania as a photocatalyst is very sensitive to its crystal phase, particle size, crystallinity, specific area, and pore structure. Since its first preparation of through a modified sol–gel process using a phosphate surfactant by David and Jackie [23] in 1995, mesoporous TiO<sub>2</sub> has received increasing attention because of numerous activated sites. This property facilitates photocatalysis in the degradation of contaminants such as humic, phenolic compounds, pesticides, chlorinated compounds, and dyes [24–29]. Thus, the synthesis and practical application of mesostructured TiO<sub>2</sub> immobilized on porous CFs in photocatalytic processes is desirable. Notwithstanding, there are few investigations on the preparation and photocatalytic efficiency of ordered mesoporous TiO<sub>2</sub> (OMT)-coated CFs (OMT/CFs). Additionally, a thorough understanding of the synergy on adsorption and photocatalysis is very important in the design and application of efficient photocatalytic systems. The synergistic effect between support and oxide mentioned above can be conventionally estimated quantitatively by synergistic factor (R) from the ratio of apparent rate constants of pure catalyst and its composites [2,4,5].

$$R = k_{app}(\text{pure oxide}) / k_{app}(\text{mixture or composites}) \quad (1)$$

However, the absence of a synergistic effect in the photocatalysis was reported in some articles mainly due to photocatalytic system without the same standard of comparison and errors usage of kinetic equation [1,4]. The latter was erroneously based on the first-order form of the approximated Langmuir–Hinshelwood (L–H) equation [2] as follow:

$$-\frac{dC}{dt} = \frac{k_r K_{ads} C}{1 + K_{ads} C} = k_r K_{ads} C = k_{app} C \quad (2)$$

where  $k_{app}$  is the apparent first-order rate constant,  $k_r$  is the reaction rate constant ( $\text{mg} \cdot \text{L}^{-1} \cdot \text{min}^{-1}$ ),

$K_{ads}$  is the equilibrium constant for the adsorption of the molecule on the catalyst surface ( $L \cdot mg^{-1}$ ). Apparently,  $k_{app}$  is greatly affected by the adsorption capacity of the catalysts. Therefore, it does not accurately evaluate synergistic effect. Additionally,  $k_{app}$  within the framework of the L–H mechanism corresponds to the case of limited adsorption wherein  $K_{ads}C \ll 1$ , so the synergistic effect estimated by using  $k_{app}$  is inaccurate. To eliminate the effect of catalyst adsorption on  $k_{app}$  and to accurately evaluate synergistic effect, the kinetic model with a rate constant which excludes the influence of adsorption and describes the photocatalytic behavior is thus required. However, little experimental information concerning the evaluation of synergy has been available so far.

In the present work, OMT was supported on CFs (OMT/CFs) by a combined method of supercritical deposition and liquid crystal template (LCT) technique. To verify the existence of the the high photocatalytic activity of OMT/CFs and establish correct evaluation of synergistic effect, we also use sol-gel method to prepare nanostructure titania on carbon fibers (NST/CFs) as comparison. Acid orange 7 (AO7;  $C_{16}H_{11}N_2O_4SNa$ ), an anionic monoazo organic compound widely used in dyeing and textile industries [30,31], was used as a model of hydrosoluble phenylazonaphthol dyes to evaluate photocatalyst performance because of its resistance to biological degradation.

## 2. Experimental

### 2.1. Reagents

Raw carbon fibers were used as supports, prepared by spinning of polyacrylonitrile and obtained from Hunan East Grand Reagent Company. Tetra-*n*-butyl titanate, hydrochloric acid, absolute ethanol and cetyltrimethylammonium bromide were all analytical grade and were purchased from Beijing Zhonglian Chemical Reagent company. The chemical structure of AO7 (Biochemical Reagent, Shanghai Jufeng Chemicals) and its absorption spectrum are given in Fig.S1. Deionized water, purified with an Elga-Pure water purification system, was used to prepare all solutions for the

experiments.

## 2.2. Preparation of photocatalysts

OMT/CFs were prepared by deposition in supercritical CO<sub>2</sub>, using tetra-*n*-butyl titanate and liquid crystal as the precursor and soft template, respectively. First, 5 g of cetyltrimethylammonium bromide was accurately weighed and then completely dissolved in 30 mL of distilled water to form hexagonal LCTs by stirring for a specified period of time. Next, 25 mL of Tetrabutyl titanate was dissolved in 50 mL of ethanol, and the mixture was then stirred for 2 h (100 rpm) with a magnetic stirrer. Ambient laboratory temperature (20 °C) was maintained while stirring. A solution containing 3.33 ml of 35% HCl and the obtained liquid crystal was added dropwise for over 1 h until a liquid crystal sol was obtained. After the sol was aged for 12 h at room temperature, it was deposited on CFs in moderately supercritical CO<sub>2</sub>. Subsequently, organic material in the resulting composite was extracted in a Soxhlet apparatus for 48 h. The composites were dried for 30 min at 100 °C in an oven, and then calcined at 500 °C for 1 h in a nitrogen atmosphere to synthesize OMT/CFs. Simultaneously, the aged sol was also calcined at 500 °C for 1 h to synthesize pure OMT powders for comparison. To further evaluate the synergistic relationship between OMTs and CFs, and determine the effect of OMTs on the synergy, we also use sol-gel method to prepare titania particles on carbon fibers (NST/CFs) without LCT. The detailed process of the titania-sol synthesis is described in the literature [31].

## 2.3. Characterization of the composite photocatalyst

The profile of the OMT/CF photocatalyst was observed by scanning electron microscopy (SEM) (Hitachi S3400N, Japan). High-resolution transmission electron microscopy/selected area electron diffraction, (HRTEM/SAED) was performed on a JEOL (JEM 2100F) microscope. Small-angle X-ray scattering (SAXS) measurements were taken on a Nanostar U small-angle X-ray scattering

system (Bruker, Germany) using Cu  $K_{\alpha}$  radiation (40 kV, 35 mA). Wide-angle X-ray diffraction (WAXRD) patterns were recorded on a Bruker D4 X-ray diffractometer with Ni-filtered Cu  $K_{\alpha}$  radiation (40 kV, 40 mA). Nitrogen adsorption–desorption isotherms were used to determine the Brunauer–Emmett–Teller (BET) surface area and pore size distribution (ASAP2010, Micromeritics Company, USA) at 77 K. Ultraviolet–visible (UV–vis) adsorption spectroscopy measurements were performed at 298 K by using a UV–vis diffuse reflectance spectrophotometer (Shimadzu UV-2100). Photoluminescence (PL) emission spectra were measured using a Spex 500 fluorescence spectrophotometer with 325 nm radiation for excitation. The chemical states of samples were determined using X-ray photoelectron spectroscopy (XPS) (VG Scientific ESCALAB Mark spectrometer, England, Mg  $K_{\alpha}$  radiation, 1253.6 eV). The CF-supported composite was ignited at 900 °C and the TiO<sub>2</sub> loading was calculated in terms of ash weight by thermogravimetric analysis (WCT-2C, Optical Instrument Factory, Beijing).

#### 2.4. Photocatalytic reactor and light source

Experiments were carried out using a cylindrical batch reactor (8 cm diameter and 15 cm height) fitted with a 6 cm diameter water-cooled quartz jacket, which maintained the system temperature by water cycling. The main component of the system was the reactor, and an air-sparging motor stirring the reaction mixture. A 120 W UV lamp was positioned inside a Pyrex cell. The wavelength range and peak wavelength of the UV lamp were 320–400 and 365 nm, respectively.

#### 2.5. Experimental procedure and analysis

AO7 is chosen as a model organic compound to evaluate the photoactivity of the prepared samples. A known amount of AO7 (Biochemical Reagent, Shanghai Jufeng Chemicals) was dissolved in deionized water to a concentration of 1 mg•L<sup>-1</sup>. The dosage of OMT/CFs in the solution was maintained within 1g•L<sup>-1</sup> at pH 7. The experimental procedure involved placing 500 mL of the

filtered suspension in the photocatalytic reactor. Air was bubbled through the reaction solution at a flow rate of  $560 \text{ mL min}^{-1}$  to ensure a constant concentration of dissolved oxygen. Thereafter, a sample of about 5 mL was withdrawn at a specific time interval of illumination and then filtered through 0.45 mm filters. The AO7 concentration in the reaction mixture was monitored in a TU-1810 spectrophotometer by measuring the absorption intensity at  $\lambda_{\text{max}}$  of 480 nm in a 10 mm quartz cell. Calculations were done using a calibration curve.

### 3. Results and discussion

#### 3.1. Morphological and textural properties of OMT/CFs

The morphology of the obtained product was first examined by SEM. Representative SEM images of the samples are shown in Fig. 1. Compared with the original CFs (Fig. 1a), OMT/CFs (Fig. 1b) and NST/CFs (Fig. 1c) exhibited similar morphology comprising aggregates with dimensions of

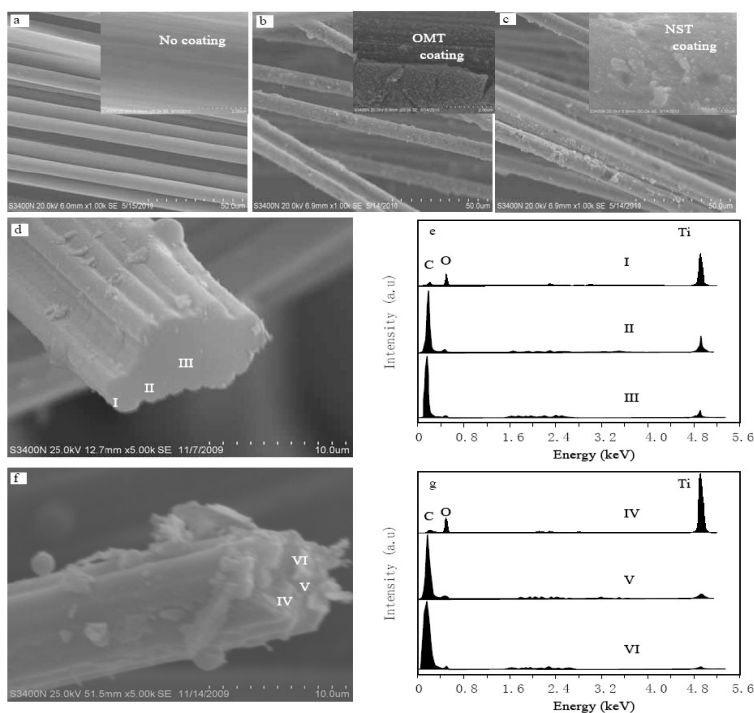


Fig.1. SEM images of carbon fibers (a), OMT/CFs (b), its cross-section (d) and corresponding EDX (e), NST/CFs (c), its cross-section (f) and corresponding EDX (g).

0.5–1.0  $\mu\text{m}$ . The aggregates consisted of smaller primary particles with irregular shapes. The titania layer had been immobilized onto almost each fiber. Although the titania layer was deposited on fibers at such a large scale, the same spatial distribution of CFs was retained by the composite. Therefore, adequate UV irradiation could penetrate the felt-form photocatalyst to a certain depth and form a three-dimensional environment for the photocatalytic reaction. This feature differentiates the present photocatalyst from current immobilized photocatalysts such as  $\text{TiO}_2$  immobilized on the surfaces of glass [32], steel plate [33], and ceramic membranes [34], which could only provide a two-dimensional surface for photodegradation. The NST/CFs showed a morphology different from that of OMT/CFs, as well as relatively large aggregates consisting of larger particles with cubic, round, and rectangular shapes (insets, Fig. 1b and c). These features are due to the excess NST particles coated on the surface of CFs by the sol-dipping–gel method. Nevertheless, the titania loadings of both composites were almost the same (15.2 wt%), which is determined by TG-DTA. To verify this, EDX spectrometry was performed on a cross-section of OMT/CFs at three different regions: I, II, and III (Fig. 1d). Results are presented in Fig. 1e. Greater amounts of Ti and O were present in the lateral regions, but as the EDX probe entered deep into the fibers, the percentage of Ti and O detected decreased markedly. For example, in the wall (region I), the amount of Ti was ~54 wt%, but it declined to ~8 wt% in region II and only ~3 wt% near the center (region III). Compared with similar regions of OMT/CFs, the weight percentage of Ti in the cross-section of NST/CFs (Fig. 1f) gradually decreased from 67 wt% (region IV) to 4 wt% (region V), and then to 0.4 wt% (region VI), as shown in Fig. 1g. As expected, OMT nanoparticles not only deposited on the surface, but also in the pores of CFs. It is mainly attributed to the fact that the titania entered into the CFs more easily by supercritical deposition than by the sol-dipping–gel method.

The morphology and mesoporous structure of the obtained samples were further confirmed by

TEM observations (Fig. 2). As shown in Fig. 2a, OMT/CFs exhibit well-ordered hexagonal channel arrangement in large domain, corresponding to the SAXS pattern (later discussion). The inset of Fig.

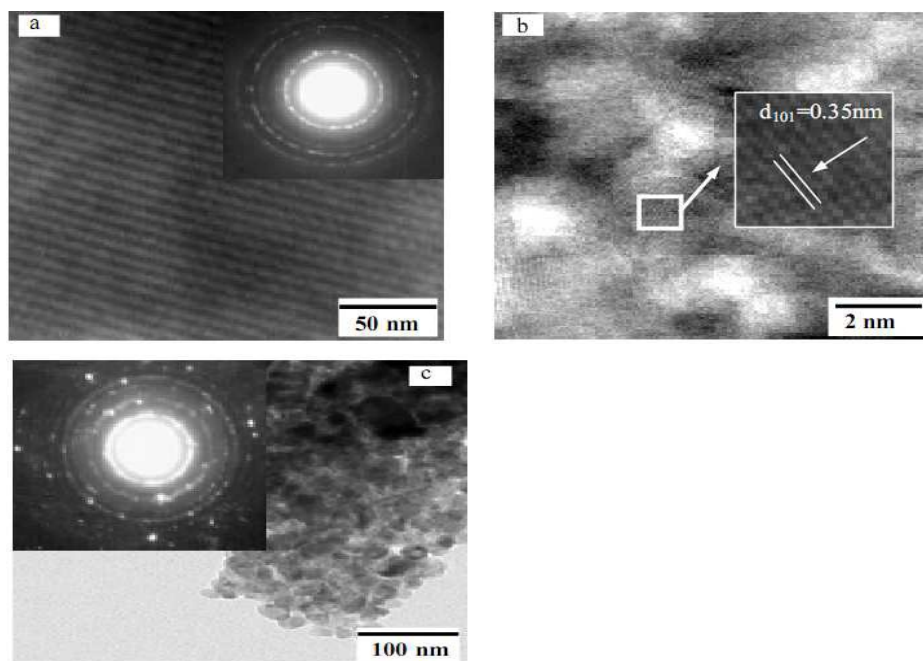


Fig.2. TEM image of OMT/CFs (a) and its HRTEM image (b) and NST/CFs (c) calcinated at 400°C.

The insets of (a, b) are selected area electron diffraction (SAED) patterns.

2a shows the SAED pattern, which also presents well-resolved diffraction rings and many diffraction spots, indicating the high crystallinity of pure anatase phase. The HRTEM images (Fig. 2b) show a 2D hexagonal mesostructure, which possesses highly ordered mesopores of about 3 nm in diameter. And the randomly oriented anatase nanocrystals with well-defined lattice planes corresponding to the (101) ( $d_{101} = 0.35$  nm) crystallographic planes of anatase. In comparison with those of OMT/CFs, NST/CFs showed larger aggregates composed of large granules of about 25 nm diameter, as seen in the TEM image (Fig. 2c). Meanwhile, the nonporous structure of the NST/CFs can be clearly recognized in the image. And the SAED pattern (inset, Fig. 2c) also suggests high crystallinity of the anatase phase, as evidenced by the well-resolved diffraction rings and numerous diffraction spots.

### 3.2. Crystalline structure of samples

For OMT and its composites, determination of the ordered pore structure was based on SAXS measurements in the  $2\theta$  range of 0.2–1.5 (Fig. 3a). The SAXS patterns of both OMT and the

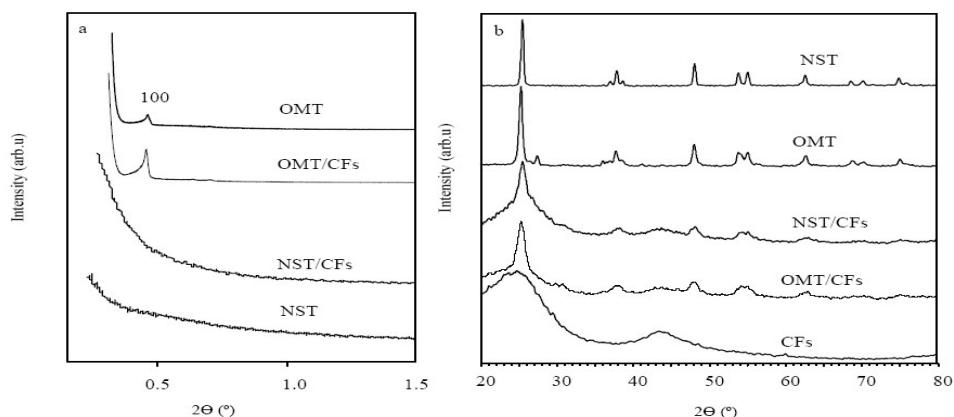


Fig.3. SAXS (a) and WAXRD (b) patterns of samples.

OMT/CFs show the characteristic Bragg peaks (reflections 100) that indicate the highly ordered hexagonal pores of the samples with similar unit cell parameters of about 10 nm. These results also suggest the composites possessed a highly organized mesoporous structure primarily attributed to the pore-forming role of the liquid crystal template in calcination process. NST and its composites did not show any diffraction peaks in the  $2\theta$  range of 0.2–1.5 in their SAXS patterns because of their extremely large pore dimensions [12]. WAXRD patterns for the OMT/CFs at a calcination temperature of 500 °C indicate only the anatase phase (Fig. 3b). The coexistence of anatase and rutile phases in pure OMT at the same calcination. It is attributed to CFs can suppress phase transformation of  $\text{TiO}_2$  from anatase to rutile structure at high temperatures [17,19]. However, such coexistence leads to lower thermal stability compared with that of pure NST without rutile. Although the patterns of OMT/CFs exhibit narrower and more intense diffraction peaks than those of raw CFs, the coexisting  $\text{TiO}_2$  peaks for NST/CFs are more distinct. The intensified anatase diffraction peaks of (101), (004), (200), (105), (211), and (204) planes for NST/CFs were observed at  $2\theta = 25.48^\circ, 37.98^\circ, 48.28^\circ, 54.28^\circ, 55.38^\circ,$  and  $64.37^\circ$  (JCPDS No. 21-1272), respectively. Meanwhile, there were

obvious decreases in the intensity of distinct diffraction peaks of CFs at G(002) ( $2\theta = 24.47^\circ$ ) and G(101) ( $2\theta = 44.29^\circ$ ) planes, suggesting the presence of numerous titania nanoparticles on the

Table 1 An overview of the texture parameters of OMT and NST supported on CFs with pure OMT, NST and their physical mixture with CFs.

Samples	Content of TiO <sub>2</sub> (wt.%) <sup>a</sup>	Surface area (m <sup>2</sup> /g) <sup>b</sup>	Total pore volume (cm <sup>3</sup> /g) <sup>c</sup>	Average pore diameter (nm) <sup>c</sup>	Crystalline size (nm) <sup>d</sup>
OMT/CFs	15.2	673	0.06	1.7	12.6
NST+CFs	15.2	1080	–	–	21.8
OMT	100	125	0.02	2.5	18.5
NST/CFs	15.2	173	0.05	3.0	16.4
OMT+CFs	15.2	1245	–	–	18.5
NST	100	53	–	–	21.8

<sup>a</sup> TiO<sub>2</sub> content was calculated by TG with an error of less than 1%.

<sup>b</sup> The BET surface area was determined by the multipoint BET method.

<sup>c</sup> The total pore volume and average pore size were calculated by the Barrett Joyner Halenda method.

<sup>d</sup> The average crystalline size of TiO<sub>2</sub> was determined by XRD using the Scherrer equation.

surface of the support. The crystallite sizes, as calculated from the broadening of the (101) anatase peak by the Scherrer equation, were found to be 12.6 nm (OMT/CFs), 18.5 nm (OMT), 16.4 nm (NST/CFs) and 21.8 nm (NST) (Table 1). The crystallite sizes of OMT/CFs and OMT are smaller than those of NST/CFs and NST, respectively. It may be attributed to the hindering effects of carbon adsorption and LCT decomposition on the growth of the anatase nanocrystals.

### 3.3. Pore structure of samples

The N<sub>2</sub> adsorption–desorption isotherms of NST and OMT/CFs as well as isotherms of pure OMT and original CFs (Fig. 4) were used in the study. Table 1 presents the surface area, pore volume, and average pore diameter of the samples and CFs. OMT exhibited a typical type IV isotherm (IUPAC classification) with well-defined capillary condensation steps, which is characteristic of OMT-type materials (Fig. 4a) [20,21]. Additionally, the shapes of the isotherms were different from one another. The pore volume of CFs was filled below a relative pressure of about 0.2, and kept almost constant at higher relative pressure; this behavior indicates that they have a highly

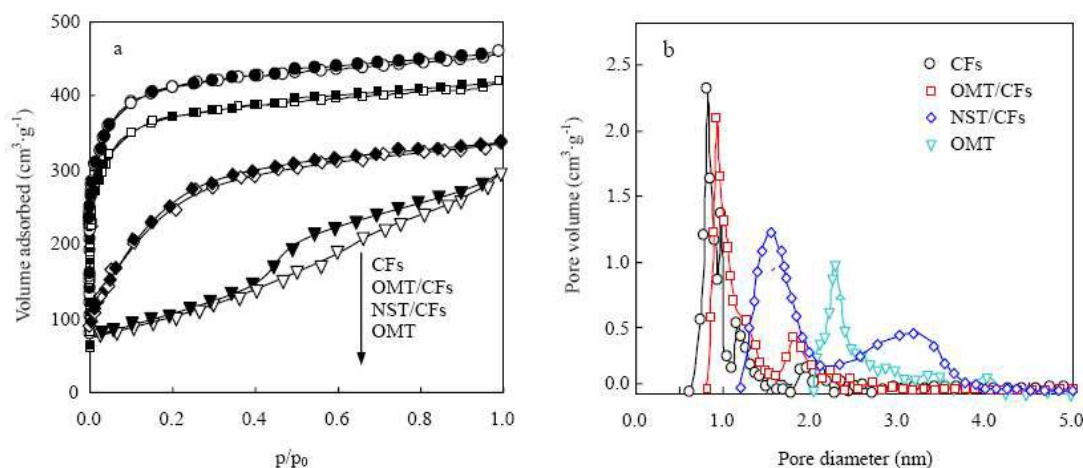


Fig.4. Nitrogen adsorption–desorption isotherms (a) and pore size distribution plots (b) of samples.

microporous structure. Filling of the pore volume of OMT/CFs took place at high relative pressure as well as below a relative pressure of about 0.2, implying that the pore channels might be blocked. The blockage might be due to growth of titania nanocrystals into the pore channels. Consistent with the results of EDX analysis, OMT particles not only deposited on the surface, but also in the pores of CFs. The NST/CFs produced isotherms that are obviously different from those of OMT/CFs at  $>0.2$  filling pressure of the pore volume. The porous nature of the sample is illustrated most graphically by the pore size distribution calculated from the adsorption isotherms, as illustrated in Fig. 4b. The distribution of OMT/CFs is broader than that of NST/CFs. However, compared with that of OMT/CFs (corresponding to about 1.7 nm), NST/CFs exhibited a relative large mean pore size (about 3.0 nm), probably because of the presence of more titania nanocrystals on the CF surface, which clogged the pore entrances. This result is in agreement with the WAXRD and EDX measurements. Additionally, the titania coverage resulted in great reduction of the surface area and micropore volume of the CFs. OMT/CFs had a SBET of  $673 \text{ m}^2 \text{ g}^{-1}$  in comparison with NST/CFs with the same content of titania because of the ordered mesostructure of titania with high surface area.

### 3.4. UV-vis adsorption and exciton photoelectron performance of samples

Diffuse reflectance spectra of the obtained samples are illustrated in Fig. 5a. All spectra clearly show the characteristic absorption edge of anatase-form  $\text{TiO}_2$  at about 350 nm and increased

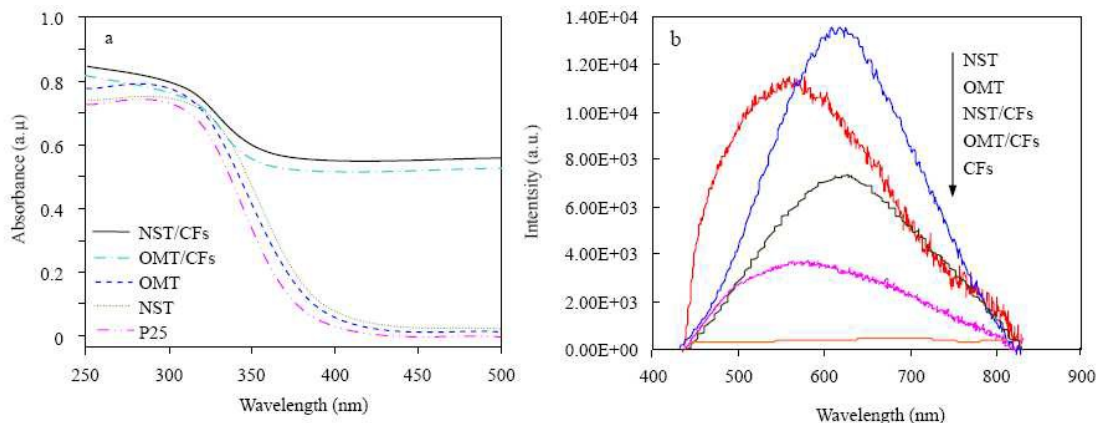


Fig.5. UV-vis diffuse reflectance spectra (a) and photoluminescence emission spectra (b) of the obtained samples.

absorbance in the UV region starting at around 350 nm. Notably, absorption intensities of the composites were higher than that pure titania at UV and visible wavelengths. This difference is mainly attributed to the black hue of CFs, and therefore the strong absorption in the entire range of wavelengths employed. There was a small shift toward longer wavelengths in the absorption band of OMT/CFs and NST/CFs, in contrast to that of pure OMT and NST, indicating that a small-particle quantum size effect was absent in the composites. The pure OMT showed a small shift toward shorter wavelengths in comparison with NST. This behavior of OMT is presumably due to its mesoporous structure and the significant surface effects. PL emission spectra of all obtained samples are shown in Fig. 5b. No luminescence of CFs was observed at 450–900 nm. The composites showed diminished PL intensity, indicating reduced charge recombination and longer-lived excitons compared with those of NST and OMT. Thus, exciton recombination could also be detrimental to the presence of CFs. Recently, similar efforts were made to combine  $\text{TiO}_2$  with CFs in simple mixtures

or as nanocomposite materials to create more highly reactive photocatalysts [15,17,19,35,36]. The PL intensity of OMT/CFs was lower than that of NST/CFs presumably because of the low content of mesoporous titania coated on surface of CFs. Additionally, OMT/CFs have high hydroxyl content in comparison with others samples according to XPS spectra as shown in Fig.S2. PL peak shifts were caused by the trapping of electrons at defect sites prior to recombination [37].

### 3.5. Adsorption isotherms

The adsorption of AO7 onto a catalyst is dependent on the surface charge, hydrophobicity, and pore structure of the catalyst, as well as on solution conditions. The amount of AO7 adsorbed at equilibrium concentration in the blank after 30 min is shown in Fig. 6a. As the equilibrium concentration of the solution increased, the amount of the adsorbed dye increased and reached a plateau. The isotherms show a typical L shape according to the classification of Charles et al. [38]. The L-shaped isotherms indicate that there was no strong competition between the solvent and the dye in occupying the catalyst surface sites [39,40]. It also implies that the localized Langmuir-type

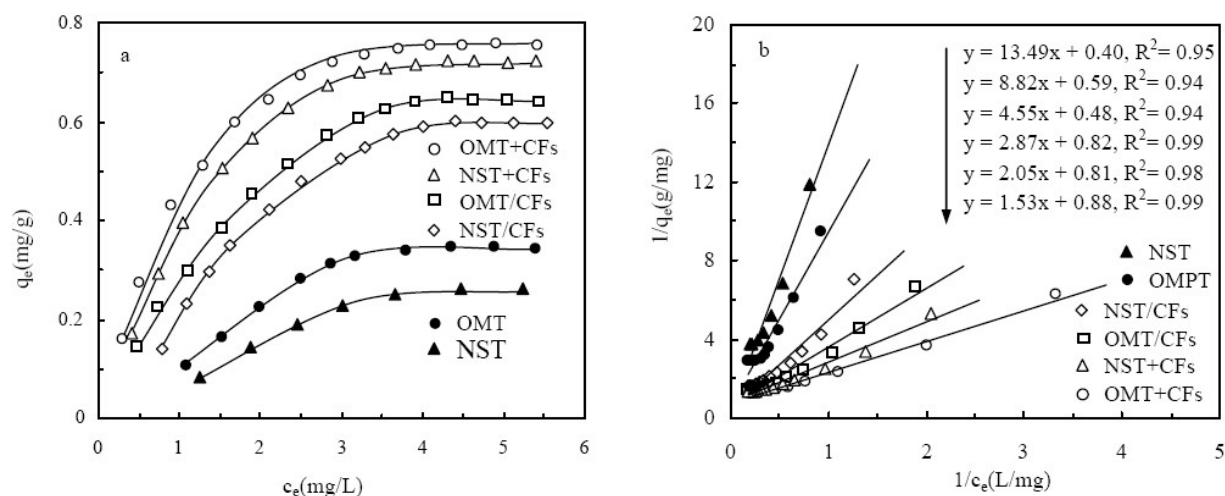


Fig.6. Adsorption isotherms (a) and relationship between  $1/c_e$  and  $1/q_e$  (b) for AO7 on the surface of catalysts.

adsorption of AO7 species in the interplane occurred in the aqueous solution/catalyst surface

interface via weak, lateral interactions [41,42]. The Langmuir isotherm constants were obtained from the plot of  $1/q_e$  against  $1/C_e$ :

$$\frac{1}{q_e} = \frac{1}{q_{\max} b C_e} + \frac{1}{q_{\max}} \quad (3)$$

where  $q_{\max}$  ( $\text{mg g}^{-1}$ ) is the maximum adsorption capacity and  $b$  is the adsorption constant related to the affinity of the binding sites ( $\text{L mg}^{-1}$ ),  $q_e$  ( $\text{mg g}^{-1}$ ) is the amount of AO7 adsorbed per unit mass of catalyst, and  $C_e$  ( $\text{mg L}^{-1}$ ) is the equilibrium concentration of unadsorbed AO7 in solution. Fitted parameters (correlation coefficient  $R^2$ ,  $b$ , and  $q_m$ ) for the linear fitted curves for the AO7 adsorption isotherms (Fig. 6b) were obtained. Values of  $b$ , which are related to the affinity of the binding sites of all samples, are listed in Table 2. Clearly, the adsorption–desorption process reached dynamic equilibrium in solution, which is affected by the various catalysts. Consistent with many reports [20,23], the affinity of the binding sites increased along with the increase in catalyst surface area, which also resulted in an increase of catalyst adsorpting capacity as followed order: OMT+CFs > NST+CFs > OMT/CFs > NST/CFs > OMT > NST.

Table 2 The constants of  $k_{app}$ ,  $k_r$ , and  $K_{ads}$  and parameter  $b$  of AO7 photodegradation with different catalysts, and corresponding  $K_{ads}/b$  and synergetic effect values by differently calculated method.

Catalysts	$k_{app}(\text{min}^{-1})^a$	$K_{ads}(\text{L/mg})^b$	$k_r(\text{mg/L}\cdot\text{min}^{-1})^b$	$b(\text{L/mg})^c$	$K_{ads}\cdot k_r(\text{min}^{-1})$	$K_{ads}/b$	SE <sup>d</sup>	SE <sup>e</sup>
OMT/CFs	0.017	0.84	0.032	0.29	0.027	2.9	5.7	2.2
OMT+CFs	0.006	0.6	0.025	0.57	0.012	1.1	2.0	1.3
OMT	0.003	0.34	0.015	0.07	0.005	4.9	1.0	1.0
NST/CFs	0.009	0.5	0.03	0.11	0.015	4.5	4.5	2.1
NST+CFs	0.005	0.37	0.024	0.32	0.009	1.2	2.5	1.4
NST	0.002	0.16	0.016	0.03	0.003	5.3	1.0	1.0

<sup>a</sup> Apparent rate constant was calculated by first-order kinetics.

<sup>b</sup> The adsorption constant and rate constant were determined by the L–H equation.

<sup>c</sup> The adsorption constant was calculated by the langmuir equation.

<sup>d</sup> The synergetic effect was determined by  $k_{app}$  ratio of composites to pure sample.

<sup>e</sup> The synergetic effect was calculated by  $k_r$  ratio of composites to pure sample.

### 3.6. Photocatalytic degradation of AO7

To evaluate the actual photocatalytic activity of the obtained photocatalysts, comparison of three AO7 processes, namely, photolysis, photolysis and adsorption of unmodified CF, and photocatalytic

decomposition by OMT/CFs and NST/CFs, was carried out, and the results are shown in Fig.7. AO7 could be slightly degraded by UV irradiation, as shown by the curve for photolysis. The curve for photolysis and adsorption on the unmodified CFs suggests that unmodified CFs had a saturated adsorptive capacity for AO7 although the adsorptive capacity was very large because of the high

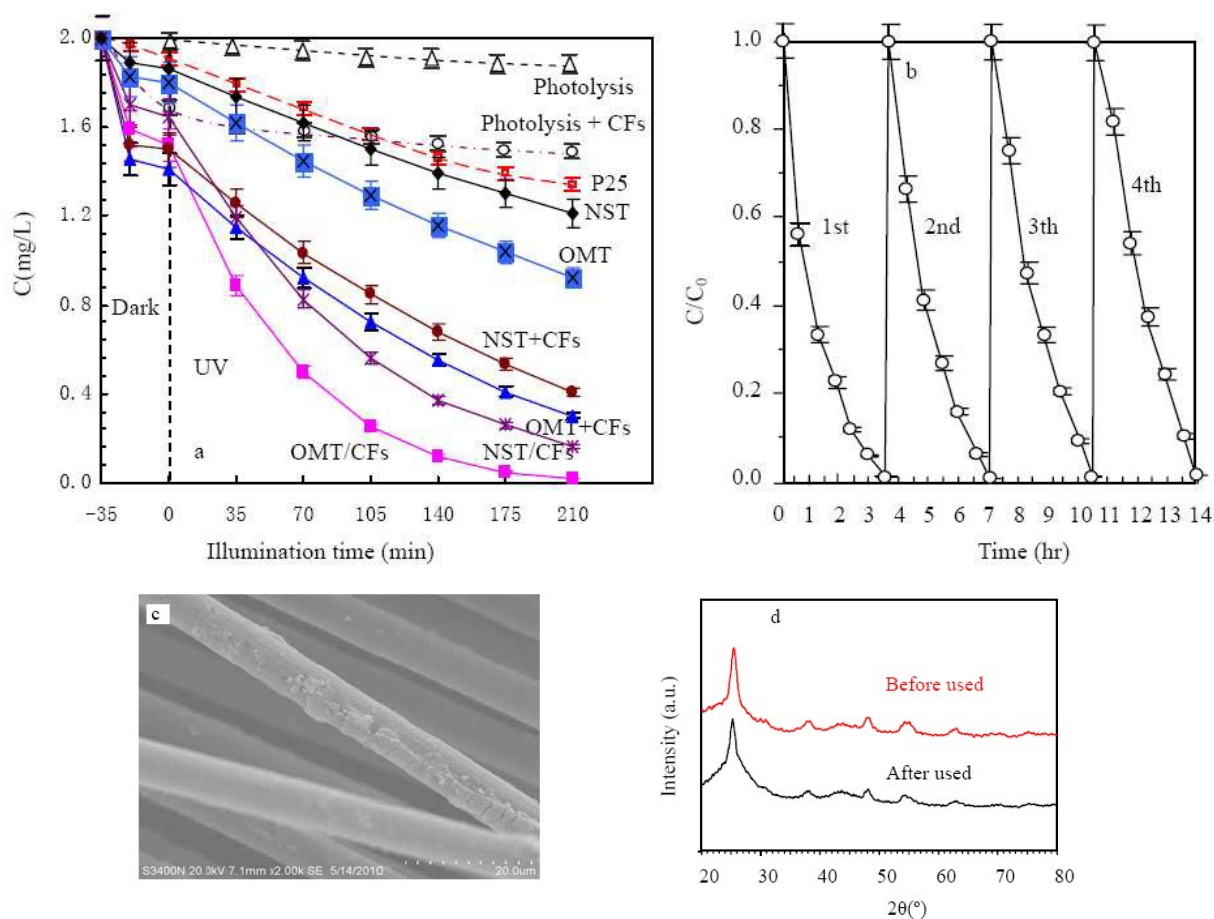


Fig. 7. Photocatalytic degradation of AO7 by the obtained samples and commercial P25 (a) and cycling runs for the photodegradation of AO7 over OMT/CFs (b), SEM image (c) and XRD patterns (d) of OMT/CFs after four cycles. ; catalyst content = 1g/l, pH = 7, AO7 content=1mg/L.

SBET of the CFs. The rate of AO7 removal via photocatalytic degradation was much higher than that via photolysis and adsorption on unmodified CFs, although the SBET of the photocatalysts were much smaller than that of the CFs. Evidently, the photocatalytic activity of P25 was lower than that of pure NST. The photocatalytic activity of OMT was greater than that of NST because of its porous

structure. The mixtures of NST, OMT, and CFs showed photocatalytic activity much higher than that of pure titania because photodecomposition of adsorbed AO7 enhanced the adsorption rate of AO7 by keeping the adsorptive capacity of the support unsaturated. Alternatively, continued adsorption of AO7 onto regenerated carbon surfaces provided the substrate for the photocatalysis of the titania layer. The improvement could be attributed to synergistic effects of factors such as crystal size of TiO<sub>2</sub>, adsorption capacity, as well as combined characteristics of carbon and titania. Furthermore, the last factor is also probably the most important, as the photocatalytic capacities of OMT/CFs and NST/CFs were better than those of OMT–CF and NST–CF mixtures, respectively, when their content of titania was almost the same (15.2 %). However, due to mesostructure of TiO<sub>2</sub> with higher surface area and more active sites, OMT/CFs shows the highest photocatalytic activity. In order to test the reuse performances of composite photocatalysts, the recycle experiment on the photocatalytic decoloration of AO7 solution is carried out. As shown in Fig. 7b, the efficiency of photocatalytic decoloration is still maintained without significant decline even after the four cycles. The excellent reuse performance of the OMT/CFs may be resulted from the good binding property between OMT layer and CFs. Only a small numbers of OMT nanosheets is flaked away from CFs after four cycles, as the arrows shown in Fig. 7c. The results of XRD pattern of OMT/CFs show no detectable difference after five cycles which further indicating the stability of OMT/CFs (Fig. 7 d).

### 3.7. Synergy between surface adsorption and photocatalysis

Langmuir–Hinshelwood (L-H) kinetics is the most commonly used kinetic model for heterogeneous catalytic processes during the photodegradation of organic contaminants in solution [7,8]. Application of this model to an ideal batch reactor produces the expression as equation (2). The integrating Eq. (2) with respect to  $C_e$  as listed in equation 4,  $C = C$  at any time  $t$ , the linearized L-H expression can be given as:

$$\ln\left(\frac{C_e}{C}\right)/(C_e - C) = k_r K_{ads} t / (C_e - C) - K_{ads} \quad (4)$$

Values of  $K_{ads}$  and  $k_r$  were obtained by linear regression of the points calculated by Eq. (4) using a least-squares best-fit procedure.

Fig. 8 a and b show the experimental kinetic data and predicted kinetics by first-order and

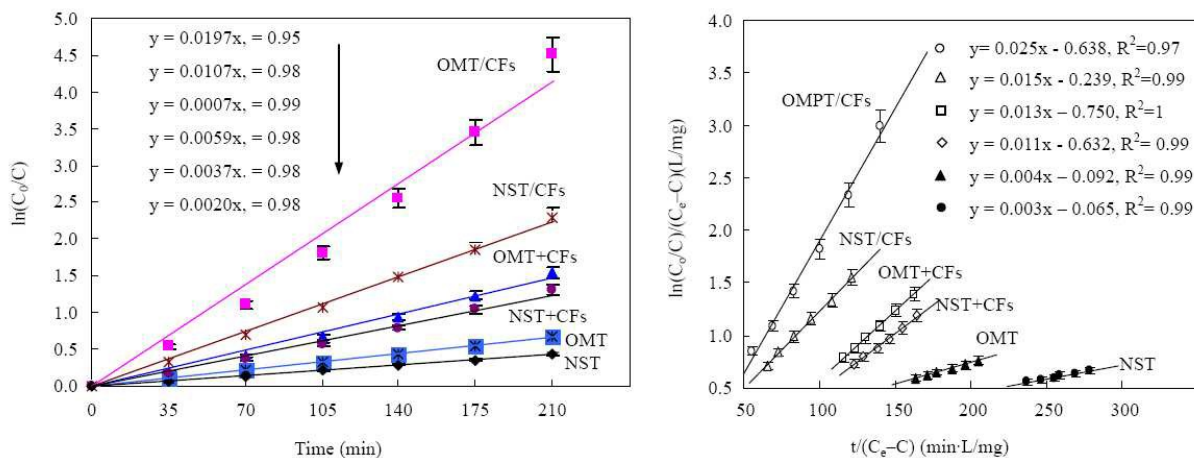


Fig.8. The AO7 photocatalytic color removal of relationship between  $\ln(C_0/C)$  and photocatalytic time (a) and the relationship between  $\ln(C_0/C)/(C_0 - C)$  and  $t/(C_0 - C)$  (b) by different catalysts with initial content of 1 g/L; PH=7, AO7 content = 1mg/L.

Langmuir-Hinshelwood kinetics by linear method, respectively. The predicted kinetic constants are shown in Table 2. The higher  $r^2$  value of equations, the better represent the AO7 degradation. It is observed that the reasonably higher  $r^2$  value for L-H kinetics for the range of initial dye concentrations suggests that it can be used to better represent the kinetics of AO7 degradation. The lower  $r^2$  values for first-order kinetics when compared to L-H kinetics suggest that it is inappropriate to represent the kinetics of photocatalysis of AO7, which is consistent with reports [2]. Additionally, as listed in Table 2, the product  $K_{ads}k_r$  calculated from the experimental values of  $k_r$  and  $K_{ads}$  in the L-H integration equation and the  $k_{app}$  value from the first-order kinetics are different among the photocatalytic systems. Both models produced different outcomes from the same experimental kinetic data. Thus, approximating the L-H kinetic expression to a first-order kinetic expression is not

appropriate. This conclusion is confirmed by the disagreement of the condition  $K_{ads}C \ll 1$ , which implies that  $K_{ads}k_r > k_{app}$  in first-order kinetics (Table 2). Thus, it is more reasonable to select  $k_r$  in L–H to represent the conventional  $k_{app}$  as a parameter to estimate the synergistic effect. To further verify this conclusion, the synergistic effect between titania and CFs, which was quantified by

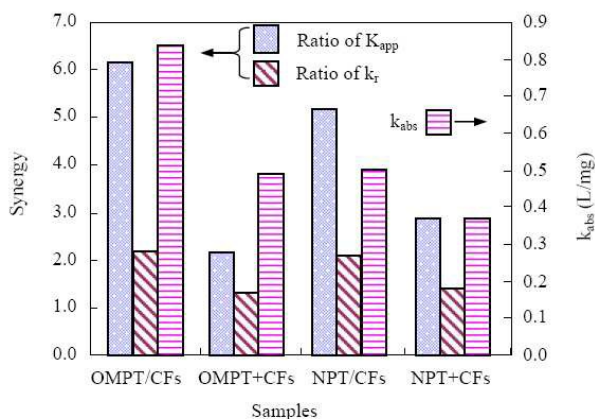


Fig. 9. Synergy calculated by ratio of  $K_{app}$  and  $k_r$  for different samples with  $k_{ads}$ .

calculating the ratios of  $k_{app}$  and  $k_r$ . As shown in Fig.9, the synergistic effect from  $k_{app}$  is greater than that from  $k_r$  because  $k_{app}$  includes  $K_{ads}$ . Both differences are more obvious for the composite catalyst because of the more adsorption contribution and higher  $k_{ads}$  (as narrated blow). Then, it is no correct for using  $k_{app}$  to evaluate synergy because all disappear of AO7 molecular not completely degraded.

### 3.8. Evidences of AO7 transfer on CFs and adsorption contribution

It was attempted to determine evidence for AO7 transfer from CFs to titania under UV-irradiation and AO7 transfer conditions for composites or mixture. The concentration of AO7 was reduced to zero by photocatalysis after different-time UV-irradiation for composites and mixtures, such as 210 min for OMT/CFs (Fig.7). Consequently, the quantity of AO7 adsorbed OMT/CFs and OMT+CFs is extracted in 5 ml acetonitrile under sonication. These values are plotted as a function of irradiation time in Fig. 10. a quantity of 0.1 and 0.13 mg of AO7 could be extracted from the OMT/CFs and OMT+CFs, respectively. It suggested that this quantity of AO7 remaining adsorbed on CFs when

AO7 was totally removed from water could undergo a photocatalytic degradation by OMT. So the

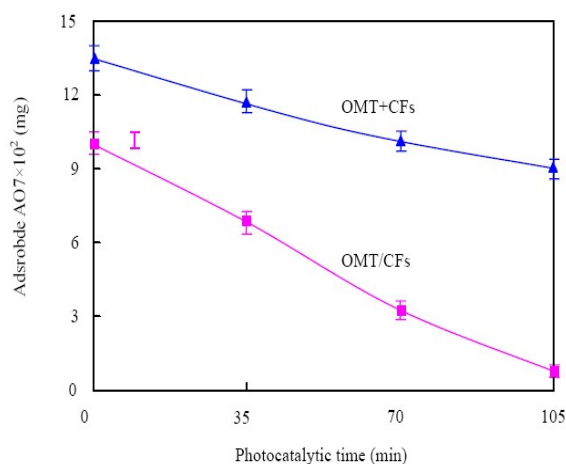


Fig.10. AO7 remaining adsorbed on OMT/CFs after total disappearance of AO7 in the solution as function of UV-irradiation time. (AO7 determined after extraction by acetonitrile.)

z result also provide the evidence that all disappear of AO7 molecules does not mean completely degradation. A photocatalysis was continue performed for different time of UV-irradiation necessary to reach a total elimination of AO7 in water. Evidently, 105 min UV-irradiation indicated that only 0.007 mg of AO7 remained adsorbed for OMT/CFs. This figure clearly illustrates that molecules of AO7 that have been adsorbed and accumulated on CFs are able to be transferred to titania where they are decomposed under irradiation. This transfer occurs through the  $\text{TiO}_2/\text{CFs}$  interface with the concentration gradient as the driving force. However, with the same photocatalytic time of 105 min, there remains 0.09 mg of AO7 adsorbed for OMT+CFs. It suggests that the adsorbed AO7 molecules easy transfer from CFs to titania due to close connection of  $\text{TiO}_2$  and CFs in composites, which is consistent with high adsorption constant ( $k_{ads}$ ) in photocatalysis. Additionally, mixture and composite of NST also present the similar phenomena as no shown in Fig.10. Meanwhile, for all samples,  $K_{ads}$  is much larger than  $b$  (see Table 2), in agreement with the results reported by Minero and Vione [43]. This may be attributed to the disequilibrium of adsorption–desorption during the

reactions due to the substantial reactivity of adsorbed active species (e.g., holes ( $h^+$ ) and radicals ( $OH\bullet$ )). These species cause continued displacement from equilibrium of the adsorbed reactant concentration, which also directly proven AO7 transfer from CFs to titania. Additionally, photocatalytic degradation of AO7 in the presence of OMT/CFs is a complex process in which adsorption and photocatalysis take place in parallel. In order to analyze the adsorption contribution to the global process, one limit case was studied. The first considers that AO7 adsorption rate was much lower than AO7 photodegradation rate. From this supposition the contribution percentage of the adsorption to the results obtained in Fig. 6 was estimated by means of the following equation.

$$\% \text{ adsorption contribution} = (C_{PT} / C_{e,PT} - C_{MC} / C_{e,MC}) / (1 - C_{MC} / C_{e,MC}) \times 100\% \quad (5)$$

Where  $C_{e,PT}$  and  $C_{e,MC}$  ( $\text{mg L}^{-1}$ ) are respective the equilibrium concentration of unadsorbed AO7 in solution by pure  $\text{TiO}_2$  and mixture or composite,  $C_{PT}$  and  $C_{MC}$  ( $\text{mg L}^{-1}$ ) are content of AO7 after degraded by pure  $\text{TiO}_2$  (PT) and its mixture or composites (MC) for the same time, respectively.

Fig. 11a shows the adsorption contribution to AO7 removal, and it is observed that: (a) CFs yielded the highest adsorptive contribution, demonstrating that the increased AO7 removal in the presence of these CFs (Fig.7) is mainly due to their adsorption capacity (Figs.6); (b) the adsorption contribution of the system was decreased as followed order: NST/CFs > OMT/CFs > NST+CFs > OMT+CFs; because the adsorbed AO7 moleculars easier transfers in composites which is consistent with the higher  $k_{ads}$  (Table 2) and experimental results of Fig.9; so adsorption contribution of composites is relatively obvious in comparison to mixtures in photocatalysis. So, evidences of AO7 transfer on CFs and adsorption contribution further exhibits inaccurate synergy between carbon fibers and  $\text{TiO}_2$  particles by the erroneous use of the first order form of the approximated L-H equation. In this sense, it also stated that  $k_{app}$  represents the disappear of AO7 moleculars in solution is not true rate constant. Additionally, adsorption contribution for NST/CFs with low surface area is higher than that for

OMT/CFs, despite that their amounts of titania were almost the same. It mainly attributed the fact that photocatalysis contribution of OMT in composites is relatively higher than that of NST. Fig. 11 b shows the adsorptive (gray bars) and photocatalytic (white bars) contributions to the AO7 removal after 210 min of treatment. It is observed that the highest adsorption contribution was clearly

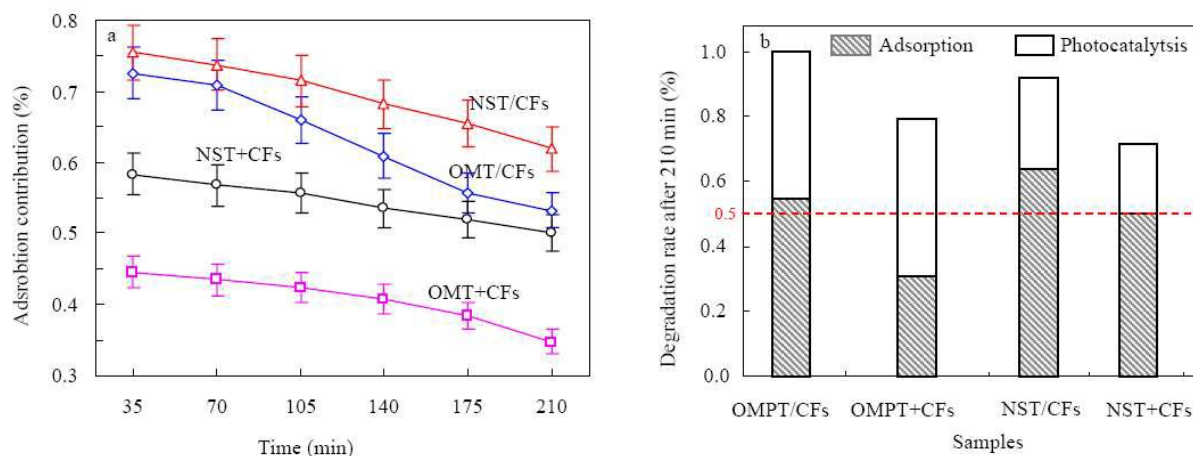


Fig.11. Adsorption contribution to AO7 removal by OMT/CFs in photocatalytic process (a) and relationship between adsorption contribution and photocatalysis contribution (b) after 210 min degradation.

obtained when using NST/CFs as catalyst, however, NST/CFs show lower photoactivity than OMT/CFs. It is important to mention that these OMT/CFs have the small crystalline size, low exciton recombination, numerous activated sites, high hydroxyl content and surface areas, which are responsible for the increase in TiO<sub>2</sub> photocatalytic activity. Additionally, this result indicates that the photocatalytic activity of the hybrid composite does not depend on the adsorption ability being the photocatalytic activity of titania the main factor influencing on the catalyst activity, in line with the study by Yang et al.[44].

#### 4. Conclusions

OMT/CFs were fabricated by a combined method of supercritical deposition and LCT technique. The OMT/CFs show the highest photocatalytic activity in AO7 degradation because of their small

crystalline size, low exciton recombination, numerous activated sites, high hydroxyl content and surface areas. Furthermore, the OMT/CFs system also exhibited good potential for commercial applications by high photoactivity of the repeating treatment of contaminated water. Photoactivities of OMT/CFs and NST/CFs were higher than those of OMT–CF and NST–CF physical mixtures because of the better synergistic effect from close combination of TiO<sub>2</sub> and CFs. The synergistic effect estimated by calculating the ratio of  $k_{app}$  from first-order kinetics is greater than that estimated by calculating the ratio of  $k_r$  from the L–H integration equation because  $k_{app}$  includes the adsorption constant. It is also proved that the decrease of AO7 content in solution is simultaneously attributed to adsorption effect of carbon fiber support besides its degradation in photocatalytic process. To eliminate the adsorption influence of the catalyst, L–H integration equation is proposed and is found to well describe the photocatalytic behavior and evaluate synergistic effect. Evidence of AO7 transfer on CFs and adsorption contribution further exhibits inaccurate synergy evaluation between carbon fibers and TiO<sub>2</sub> particles by the erroneous use of the first order form of the approximated L–H equation.

### Acknowledgments

This work has been supported by the Natural Science Foundation of China (No. 51172092), Hunan Provincial Natural Science Fund for Distinguished Young (No. 13JJ1023), and financial support of the Program for New Century Excellent Talents in Universities (No. NECT-12-0720). We appreciate the Aid program (Environment and Energy Materials and deep processing of mineral resources in Wuling Mountain ) for Science and Technology Innovative Research Team in Higher Educational Institutions of Hunan Province.

### References

[1] S. M. Miranda, G. Em. Romanos, V. Likodimos, R. R.N. Marques, E. P. Favvasc, F. K. Katsaros, K. L. Stefanopoulos, V. J.P. Vilar, J. L. Faria, P. Falaras, A. M.T. Silva, Pore structure, interface

properties and photocatalytic efficiency of hydration/dehydration derived TiO<sub>2</sub>/CNT composites, *Appl.Catal.B* 147(2014) 65–81

[2] G. A. Natalia, S. Ricardo, B.Clara, G.Marcos, Á. Patricia, M. Rosa, Correct use of the Langmuir–Hinshelwood equation for proving the absence of a synergy effect in the photocatalytic degradation of phenol on a suspended mixture of titania and activated carbon. *Carbon* 55(1)(2013) 62–69.

[3] R. Ocampo-Pérez<sup>a,b</sup>, M. Sánchez-Polo<sup>a</sup>, J. Rivera-Utrilla<sup>a</sup>, R. Leyva-Ramos, Enhancement of the catalytic activity of TiO<sub>2</sub> by using activated carbon in the photocatalytic degradation of cytarabine, *Appl. Catal. B* 104 (2011)177–184.

[4] K. Vasanth Kumar, K. Porkodi, A. Selvaganapathi, Constrain in solving Langmuire Hinshelwood kinetic expression for the photocatalytic degradation of Auramine O aqueous solutions by ZnO catalyst, *Dyes and Pigments* 75 (2007)246–249

[5] Matos J, Laine J, Herrmann JM. Synergy effect in the photocatalytic degradation of phenol on a suspended mixture of titania and activated carbon. *Appl Catal B* 18(3–4) (1998)281–291.

[6] T.H. Liou, B.C. Lai, Utilization of e-waste as a silica source for the synthesis of the catalyst support MCM-48 and highly enhanced photocatalytic activity of supported titania nanoparticles. *Appl. Catal. B* 115-116 (1) (2012)138–148.

[7] Y.J. Li, C. Liu, P. Xu, M. Li, M.X. Zen, S.H. Tang, Controlled fabrication of ordered mesoporous titania / carbon fiber composites with high photoactivity: synergistic relationship between surface adsorption and photocatalysis, *Chem. Engineer. J.* 243(2014)108–116.

[8] A. Takanobu, D. Yusuke, M. Atsushi, K. Masafumi, T. Noriaki, Y. Isao, Y. Tetsuo, First-principles calculation and proton transfer in TiO<sub>2</sub>-modified porous glass, *J. Am. Ceram. Soc.* 93 (1) (2010) 127–131.

[9] Y. Tetsuo, M. Fumiko, K. Noriaki, J. Tetsuro, Photocatalytic activity of transparent porous glass supported TiO<sub>2</sub>, *Ceram. Int.* 35 (8) (2009) 3321–3325.

[10] H.F. Guo, M. Kemell, M. Heikkil, M. Leskel, Noble metal-modified TiO<sub>2</sub> thin film photocatalyst on porous steel fiber support, *Appl. Catal. B* 95 (3-4) (2010) 358–364.

[11] L.P. Yang, A. Cai, C.Y. Luo, Z.Y. Liu, W.F. Shangguan, T.G. Xi, Performance analysis of a novel TiO<sub>2</sub>-coated foam-nickel PCO air purifier in HVAC systems, *Sep. Purif. Tech.* 68 (2) (2009) 232–237.

- [12] F.V. Leticia, B.P. José, O.A. Conchi, Phenol Adsorption and photo-oxidation on porous carbon/titania composites, *Adsorpt. Sci. Technol.* 28 (8) (2010) 727–738.
- [13] Y.H. Ao, J.J. Xu, D.G. Fu, C.W. Yuan, A simple route for the preparation of anatase titania-coated magnetic porous carbons with enhanced photocatalytic activity, *Carbon* 46 (4) (2008) 596–603.
- [14] D. Huang, Q. Liu, Y. Miyamoto, T. Matsumoto, T. Tojo, J. Ding, D. Zhang, Visible-light photoactivity of hierarchical porous carbon supported N-doped TiO<sub>2</sub>, *J. Porous. Mater.* 19 (6) (2012) 1003–1008.
- [15] A. Saha, C.M. Jiang, A. A. Martí, Carbon nanotube networks on different platforms, *Carbon*, 79(2014)1–18.
- [16] Y. Yu, M.H. Zhou, G. Xue, Z.X. Jiang, Preparation and characterization of PAN-based ultra-fine activated carbon fiber adsorbent, *J. Porous. Mater.* 18 (3) (2011) 379–387.
- [17] L. Li, P.A. Quinlivan, D.R. Knappe, Effects of activated carbon surface chemistry and pore structure on the adsorption of organic contaminants from aqueous solution, *Carbon-American Carbon Committee* 40 (12) (2002) 2085–2100.
- [18] M. Shinya, O. Akihito, H. Katsutoshi, Carbon fiber as an excellent support material for wastewater treatment biofilms, *Environ. Sci. Technol.* 46 (18) (2012) 10175–10181.
- [19] K. Shankhamala, C.N. Tharamani, X.X. Chen, W. Xia, M. Bron, W. Schuhmann, M. Muhler, Synthesis of an improved hierarchical carbon-fiber composite as a catalyst support for platinum and its application in electrocatalysis, *Carbon* 50 (12) (2012) 4534–4542.
- [20] W.X. Guo, F. Zhang, C.J. Lin, Z.L. Wang, Direct growth of TiO<sub>2</sub> nanosheet arrays on carbon fibers for highly efficient photocatalytic degradation of methyl orange, *Adv. Mater.* 24 (35) (2012) 4761–4764.
- [21] G. Xue, H.H. Liu, Q.Y. Chen, C. Hills, M. Tyrer, F. Innocent, Synergy between surface adsorption and photocatalysis during degradation of humic acid on TiO<sub>2</sub>/activated carbon composites, *J. Hazard. Mater.* 186 (1) (2011) 765–772.
- [22] S. Dutta, S.A. Parsons, C. Bhattacharjee, P. Jarvis, S. Datta, S. Bandyopadhyay, Kinetic study of adsorption and photo-decolorization of Reactive Red 198 on TiO<sub>2</sub> surface, *Chem. Engineer. J.* 155 (3) (2009) 674–679.
- [23] S.B. Alexey, V.V. Alexander, Fast elimination of organic airborne compounds by adsorption and

catalytic oxidation over aerosol TiO<sub>2</sub>, *Catal. Commun.* 9 (15) (2008) 2598–2600.

[24] M.A. David, Y.Y. Jackie, Synthese von hexagonal gepacktem, mesoporösem TiO<sub>2</sub> mit einer modifizierten Sol-Gel-Methode, *Angew. Chem.* 107 (18) (1995) 2202–2206.

[25] C.X. He, B.Z. Tian, J.L. Zhang, Synthesis of thermally stable and highly ordered bicontinuous cubic mesoporous titania–silica binary oxides with crystalline framework, *Microporous. Mesoporous. Mater.* 126 (1–2) (2009) 50–57.

[26] J.G. Yu, G.H. Wang, B. Cheng, M.H. Zhou, Effects of hydrothermal temperature and time on the photocatalytic activity and microstructures of bimodal mesoporous TiO<sub>2</sub> powders, *Appl. Catal. B* 69 (3–4) (2007) 171–180.

[27] D.S. Kim, S.J. Han, S.Y. Kwak, Synthesis and photocatalytic activity of mesoporous TiO<sub>2</sub> with the surface area, crystallite size, and pore size, *J. Colloid. Interface. Sci.* 316 (1) (2007) 85–91.

[28] T.C. An, J.K. Liu, G.Y. Li, S.Q. Zhang, H.J. Zhao, X.Y. Zeng, G.Y. Sheng, J. Fu, Structural and photocatalytic degradation characteristics of hydrothermally treated mesoporous TiO<sub>2</sub>, *Appl. Catal. A* 350 (2) (2008) 237–243.

[29] Y.C. Feng, L. Li, M. Ge, C.S. Guo, J.F. Wang, L. Liu, Improved catalytic capability of mesoporous TiO<sub>2</sub> microspheres and photodecomposition of toluene, *ACS. Appl. Mater. Int.* 2 (11) (2010) 3134–3140.

[30] K. Zimny, T. Roques-Carnes, C. Carteret, M.J. Stebe, J.L. Blin, Synthesis and photoactivity of ordered mesoporous titania with a semicrystalline framework, *J. Phys. Chem.* 116 (11) (2012) 6585–6594.

[31] B. Kyriakos, S. Maria, I.K. Dimitris, E.V. Xenophon, Adsorption of acid orange 7 on the surface of titanium dioxide, *Langmuir* 21 (30) (2005) 9222–9230.

[32] Y.J. Li, X.D. Li, J.W. Li, J. Yin, Photocatalytic degradation of methyl orange by TiO<sub>2</sub>-coated activated carbon and kinetic study, *Water. Res.* 40 (2006) 1119–1126.

[33] E. Aubry, J. Lambert, V. Demange, A. Billard, Effect of Na diffusion from glass substrate on the microstructural and photocatalytic properties of post-annealed TiO<sub>2</sub> films synthesised by reactive sputtering, *Surf. Coat. Technol.* 206 (23) (2012) 4999–5005.

[34] L. Axel, G. Thierry, P. Sébastien, B.R. Elisabeth, Catalytic coatings for structured supports and reactors: VO<sub>x</sub> /TiO<sub>2</sub> catalyst coated on stainless steel in the oxidative dehydrogenation of propane, *Appl. Catal. A* 391 (1–2) (2011) 43–51.

- [35] Y.Wang, G.H. Chen, Q.H. Shen, F.M. Zhang, G.L. Chen, Hydrothermal synthesis and photocatalytic activity of combination of flowerlike TiO<sub>2</sub> and activated carbon fibers, *Mater. Let.* 116(2014)27–30.
- [36] N. K. Dey, M. J. Kim, K. D. Kim, H. O. Seo, D.W. Kim, Y. D. Kim, D. C. Lim, K. H. Lee, Adsorption and photocatalytic degradation of methylene blue over TiO<sub>2</sub> films on carbon fiber prepared by atomic layer deposition, *J. Mol. Catal. A. Chem.* 337 (1-2) (2011) 33–38.
- [37] P. Fu, Y. Luan, X. Dai, P.F. Fu, Y. Luan, X.G. Dai, CeO<sub>2</sub>-TiO<sub>2</sub> coated ceramic membrane with catalytic ozonation capability for treatment of tetracycline in drinking water, *J. Mol. Catal. A* 221 (1) (2004) 81–88.
- [38] Y. Yao, G.H. Li, S.N. Ciston, R.M. Lueptow, K.A. Gray, Photoreactive TiO<sub>2</sub>/carbon nanotube composites: synthesis and reactivity, *Environ. Sci. Technol.* 42 (13) (2008) 4952–4957.
- [39] H. Charles, P.D. Anthony, A.E. Ian, A general treatment and classification of the solute adsorption isotherm part. II. Experimental interpretation, *J. Colloid and Interface. Sci.* 47 (3) (1974) 766–778.
- [40] B. Kyriakos, S. Maria, I.K. Dimitris, E.V. Xenophon, Adsorption of acid orange 7 on the surface of titanium dioxide, *Langmuir* 21 (2005) 9222–9230.
- [41] M. Muruganandham, M. Swaminathan, Solar photocatalytic degradation of a reactive azo dye in TiO<sub>2</sub>-suspension, *Sol. Energy. Mater. Sol. Cells* 81 (4) (2004) 439.
- [42] N. Spanos, L. Vordonis, C. Kordulis, A. Lycourghiotis, Molybdenum-oxo species deposited on alumina by adsorption: II. Regulation of the surface MoVI concentration by control of the protonated surface hydroxyls, *J. Catal.* 124 (2) (1990) 315–323.
- [43] C.H. Giles, D. Smith, A. Huitson, A general treatment and classification of the solute adsorption isotherm. I. Theoretical, *J. Colloid. Interface. Sci.* 47 (3) (1974) 755–765.
- [44] C. Minero, D. Vione, A quantitative evaluation of the photocatalytic performance of TiO<sub>2</sub> slurries, *Appl. Catal. B* 67 (2006) 257–269.
- [45] J. Yang, J. Zhang, L. Zhu, S. Chen, Y. Zhang, Y. Tang, Y. Zhu, Y. Li, Synthesis of nano titania particles embedded in mesoporous SBA-15: characterization and photocatalytic activity, *Hazard. Mater.B* 137 (2006) 952–958.

## Graphical abstract

OMT/CFs show high photoactivity due to some superiorities, and a L–H integration equation is proposed to well evaluate synergy.

